Electronic Supplementary Information

B-Site Substitution in $NaCo_{1-2x}Fe_xNi_xF_3$ Perovskites for Efficient Oxygen Evolution

Hu Yao[a], Yinan Zheng[a], Siliang Yue[a], Wenyu Yuan[b*], Xiaohui Guo[a*]

[a] Dr. Hu Yao, Yinan Zheng, Silaing Yue and Prof. Xiaohui Guo, Key Lab of Synthetic and Natural Functional Molecule Chemistry of Ministry of Education, The College of Chemistry and Materials Science, Northwest University, Xi'an 710069, P. R. China.
[b]Dr. Wenyu Yuan, Key Laboratory of Macromolecular Science of Shaanxi Province, Key Laboratory of Applied Surface and Colloid Chemistry, School of Chemistry & Chemical Engineering, Shaanxi Normal University, Xi'an 710062, P. R. China.

*Corresponding author e-mail: guoxh2009@nwu.edu.cn; wenyu.yuan@snnu.edu.cn

Table of contents

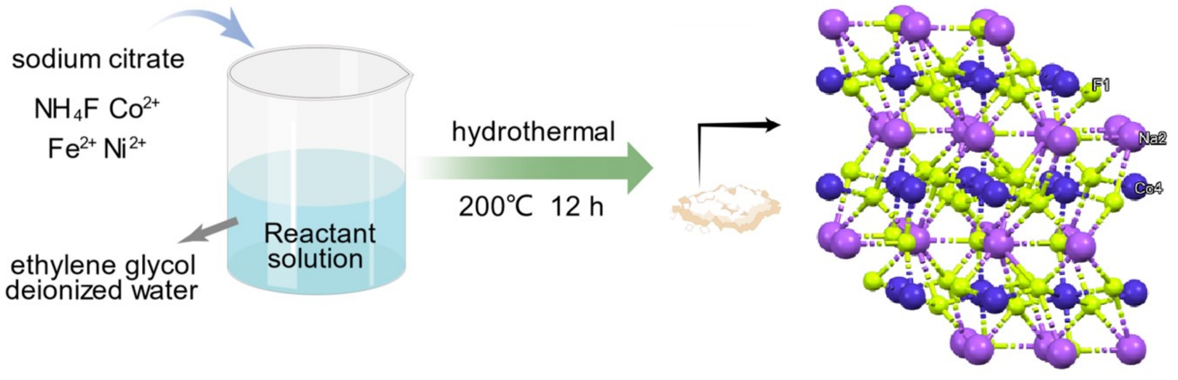

Figure S1 Illustration of the preparation process for $NaCo_{1-2x}Fe_xNi_xF_3$ (x=0/0.1/0.2/0.3) samples and crystal structure.

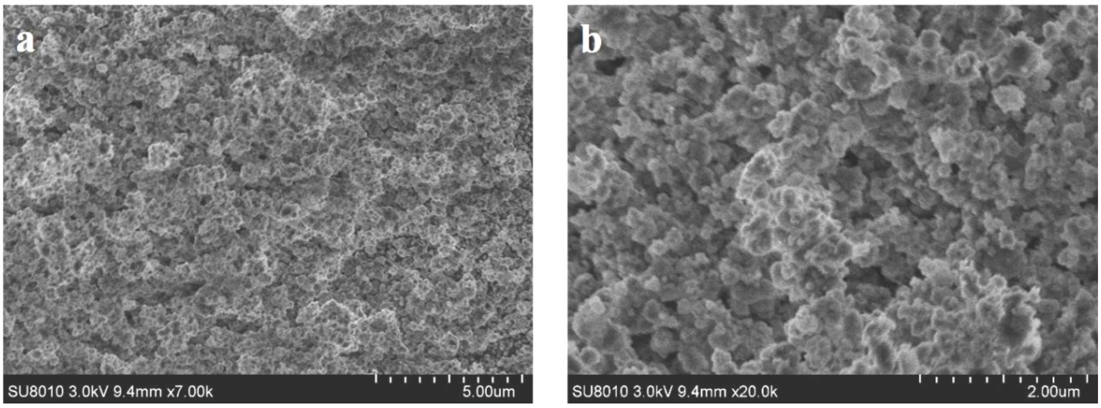

Figure S2. (a-b) SEM images of the prepared NCFNF(433).

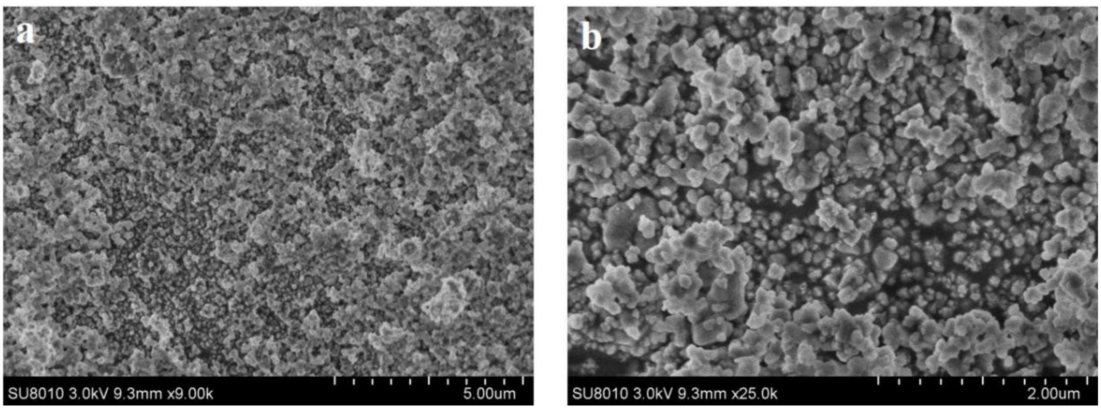

Figure S3. (a-b) SEM images of the prepared NCFNF(622).

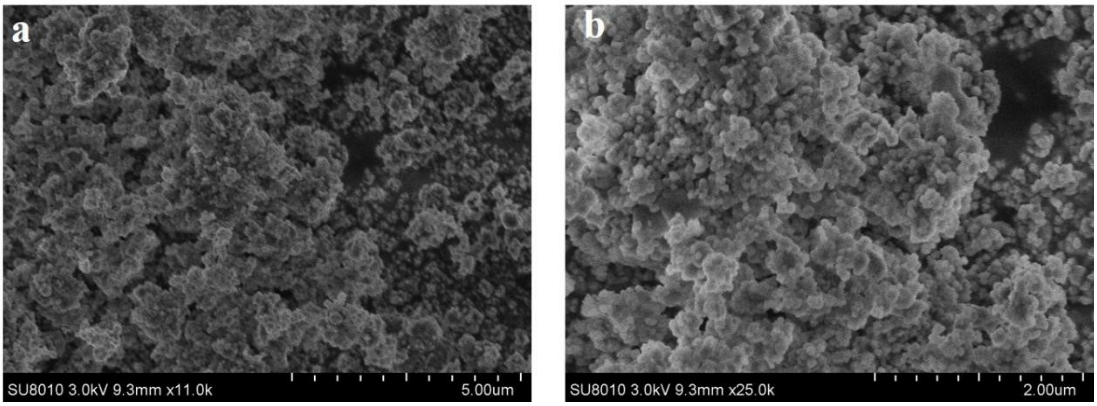

Figure S4. (a-b) SEM images of the prepared NCFNF(811).

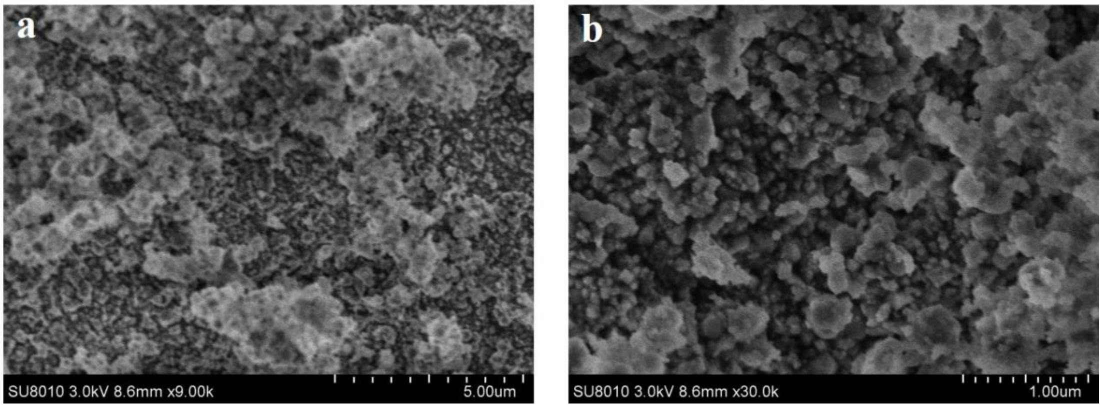

Figure S5. (a-b) SEM images of pure NCF.

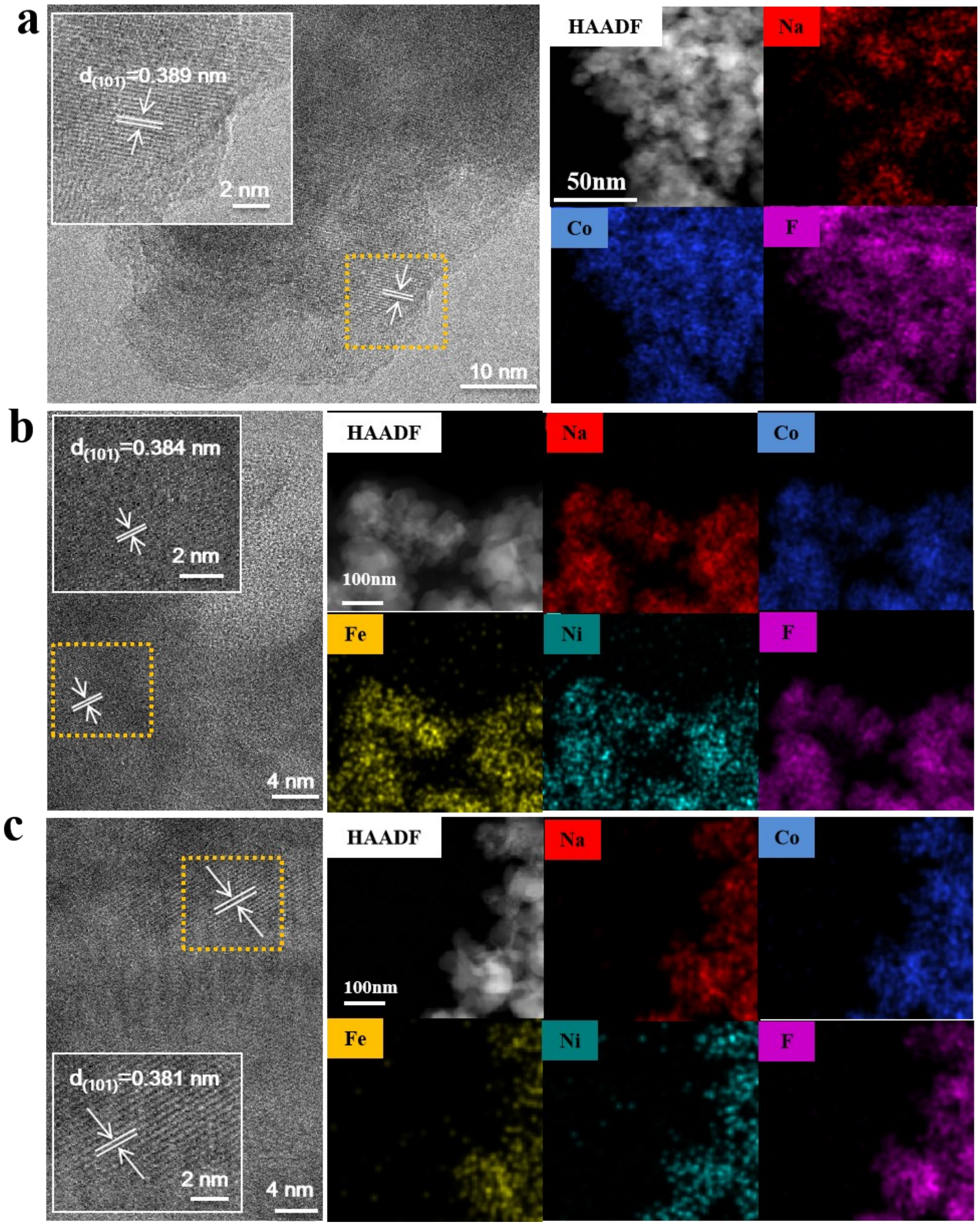

Figure S6. (a-c) HRTEM image and EDX elemental mapping of the prepared $NaCo_{1-2x}Fe_xNi_xF_3$ (x=0/0.1/0.2).

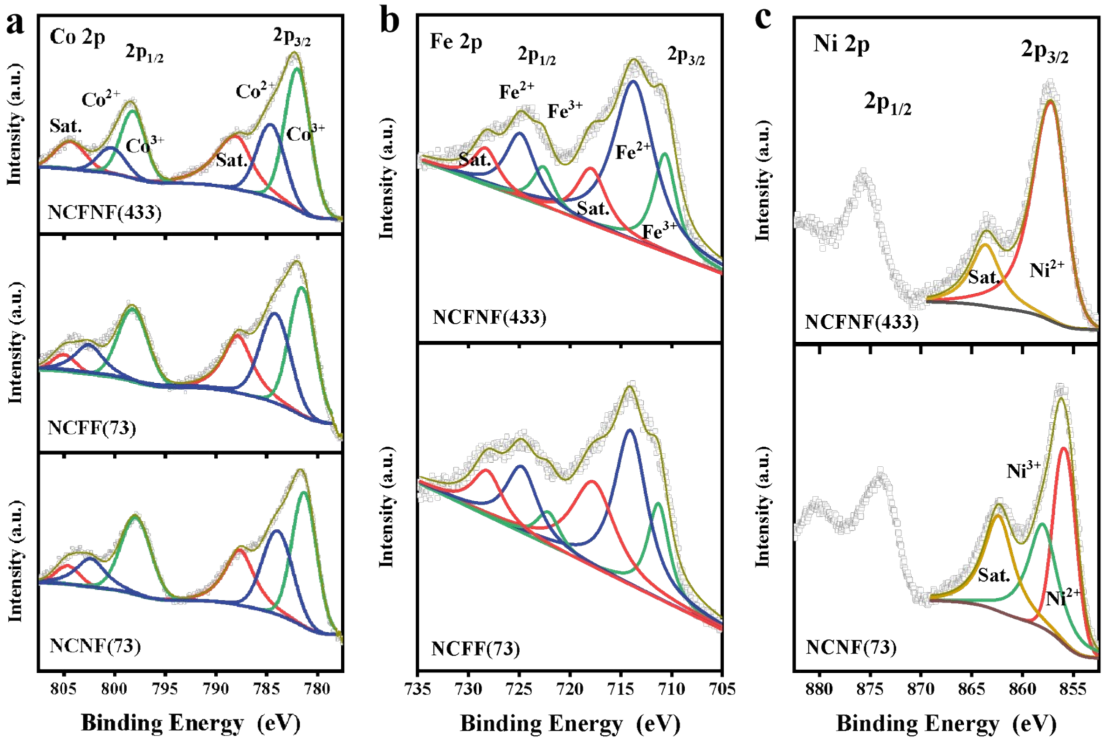

Figure S7. (a) Co 2p XPS of NCFNF(433), NCFF(73) and NCNF(73); (b) Fe 2p XPS of NCFNF(433) and NCFF(73); (c) Ni 2p XPS of NCFNF(433) and NCNF(73).

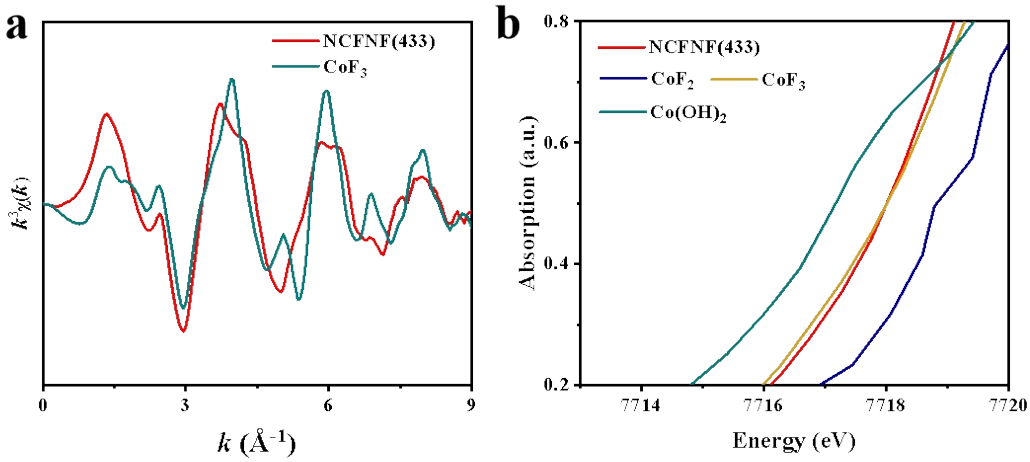

Figure S8. (a) The Co K-edge extended XAFS oscillation function of NCFNF(433) and CoF_3; (b) Co K-edge XANES of NCFNF(433), CoF_2, CoF_3, $Co(OH)_2$.

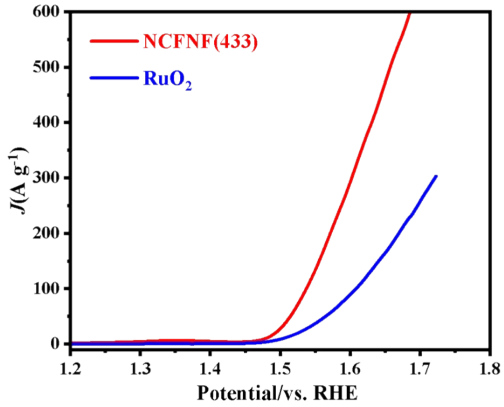

Figure S9. Mass activities plots for NCFNF(433) and RuO_2.

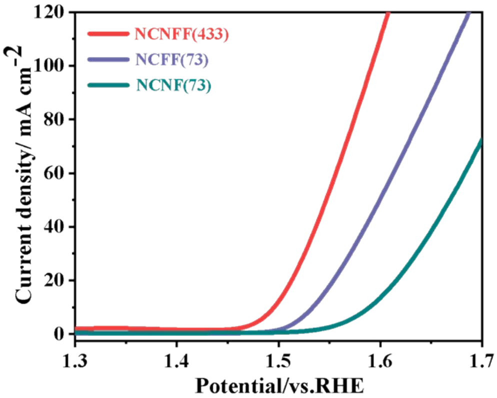

Figure S10. OER polarization curves of the fluoride perovskite series.

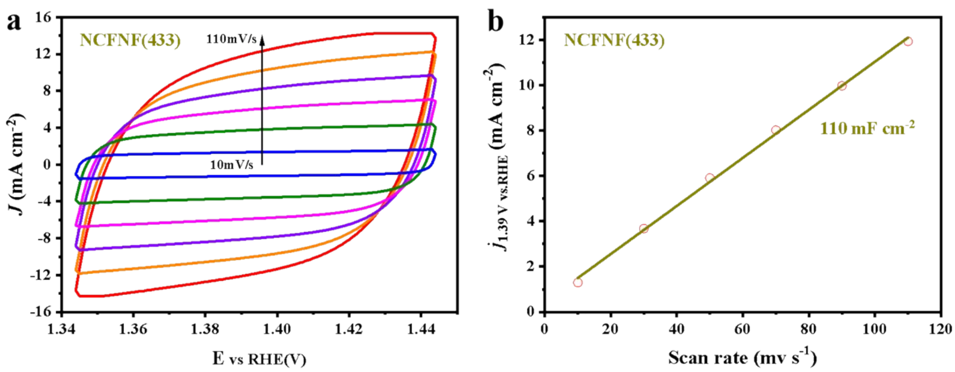

Figure S11. (a) CVs with different scan rates in a potential window (1.34-1.44 V vs RHE) for NCFNF(433). (b) Charging current density differences ($j = (j_+ - j_-)/2$) at 1.39 V vs RHE plotted against scan rates for NCFNF(433).

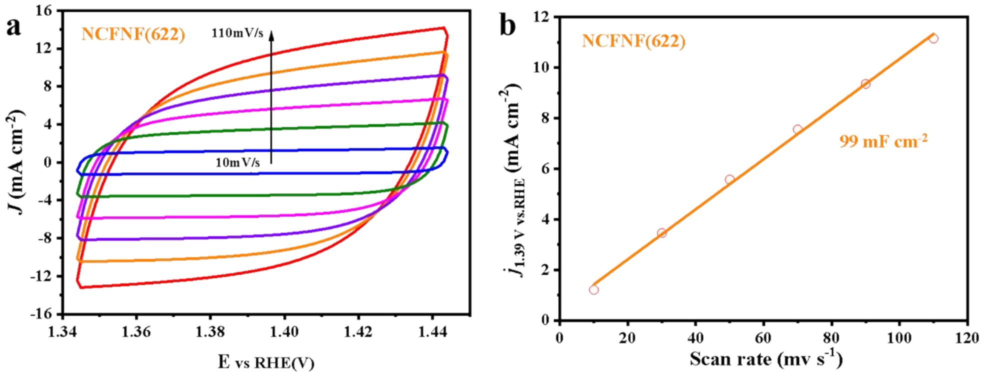

Figure S12. (a) CVs with different scan rates in a potential window (1.34-1.44 V vs RHE) for NCFNF(622). (b) Charging current density differences ($j = (j_+ - j_-)/2$) at 1.39 V vs RHE plotted against scan rates for NCFNF(622).

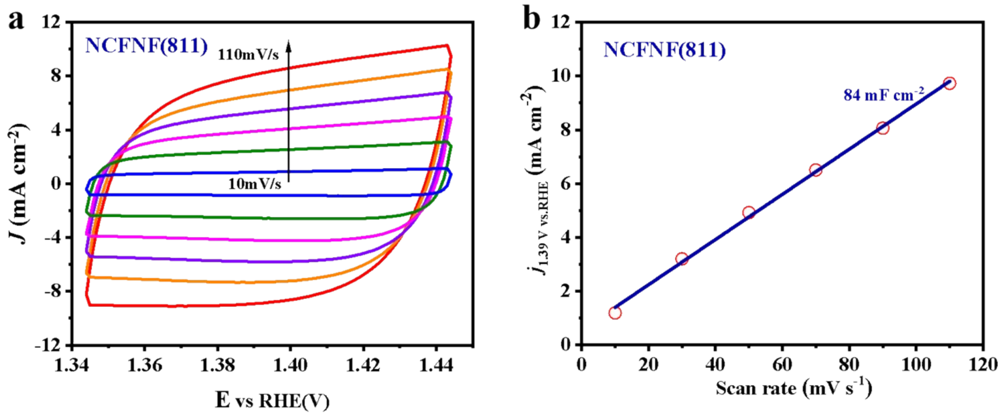

Figure S13. (a) CVs with different scan rates in a potential window(1.34-1.44 V vs RHE) for NCFNF(811). (b) Charging current density differences ($j = (j_+ - j_-)/2$) at 1.39 V vs RHE plotted against scan rates for NCFNF(811).

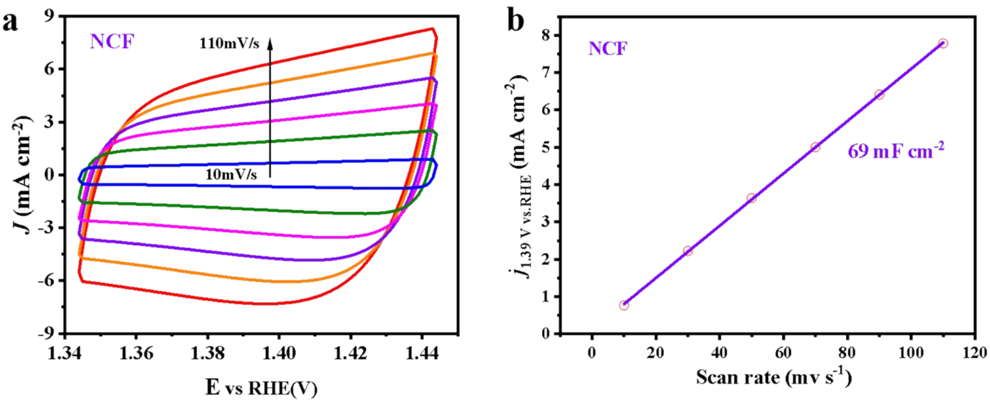

Figure S14. (a) CVs with different scan rates in a potential window (1.34-1.44 V vs RHE) for NCF. (b) Charging current density differences ($j = (j_+ - j_-)/2$) at 1.39 V vs RHE plotted against scan rates for NCF.

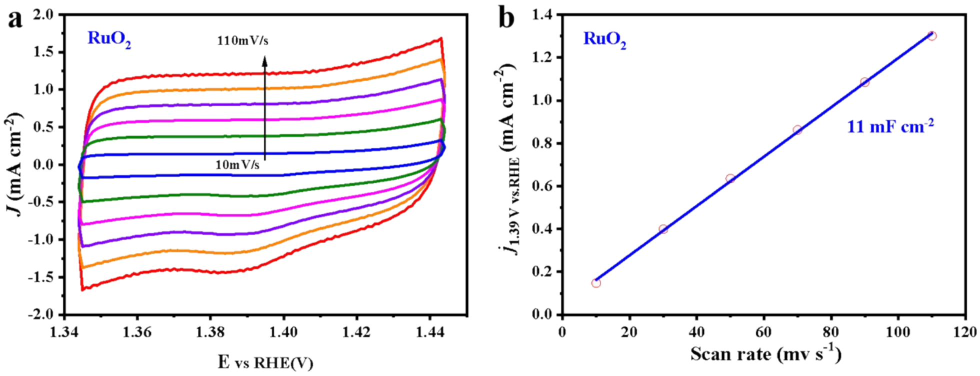

Figure S15. (a) CVs with different scan rates in a potential window (1.34-1.44 V vs RHE) for RuO_2. (b) Charging current density differences ($j = (j_+ - j_-)/2$) at 1.39 V vs RHE plotted against scan rates for RuO_2.

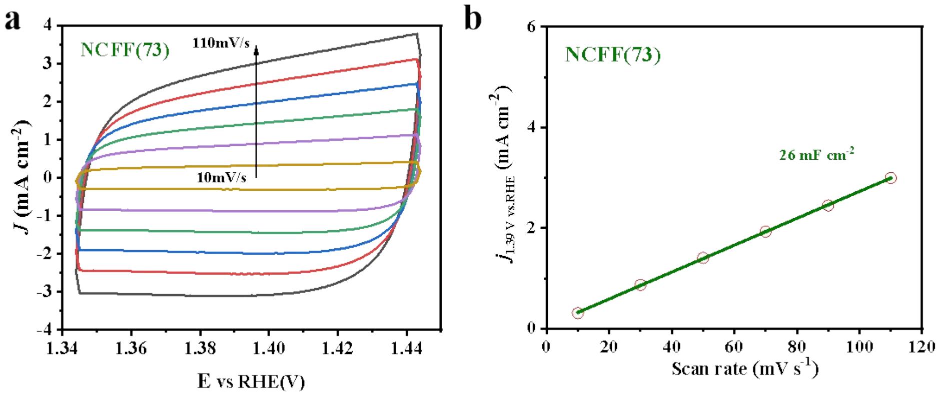

Figure S16. (a) CVs with different scan rates in a potential window (1.34-1.44 V vs RHE) for NCFF(73). (b) Charging current density differences ($j = (j_+ - j_-)/2$) at 1.39 V vs RHE plotted against scan rates for NCFF(73).

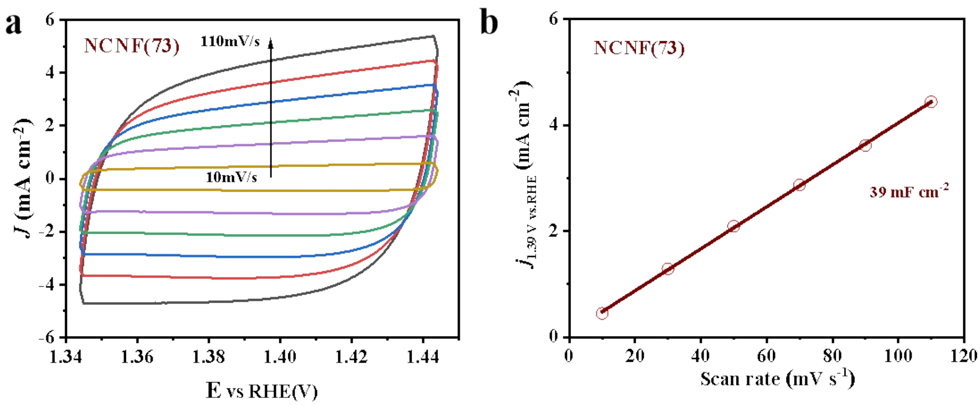

Figure S17. (a) CVs with different scan rates in a potential window (1.34-1.44 V vs RHE) for NCNF(73). (b) Charging current density differences ($j = (j_+ - j_-)/2$) at 1.39 V vs RHE plotted against scan rates for NCNF(73).

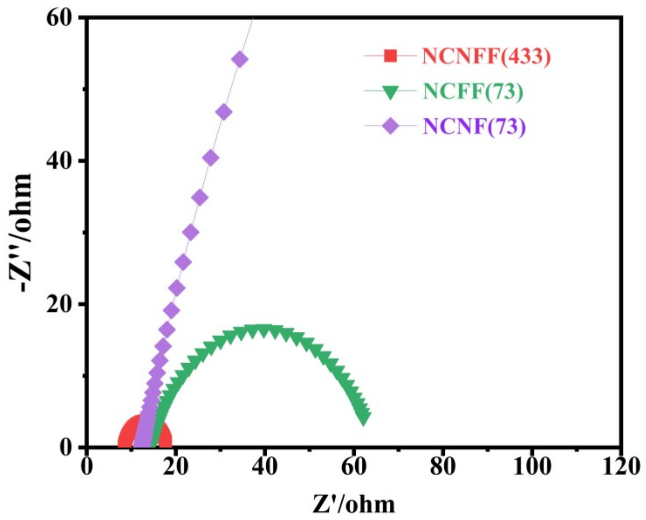

Figure S18. Nyquist plots of the catalysts in 1 M KOH at 1.524 V (vs RHE) and the corresponding equivalent circuit.

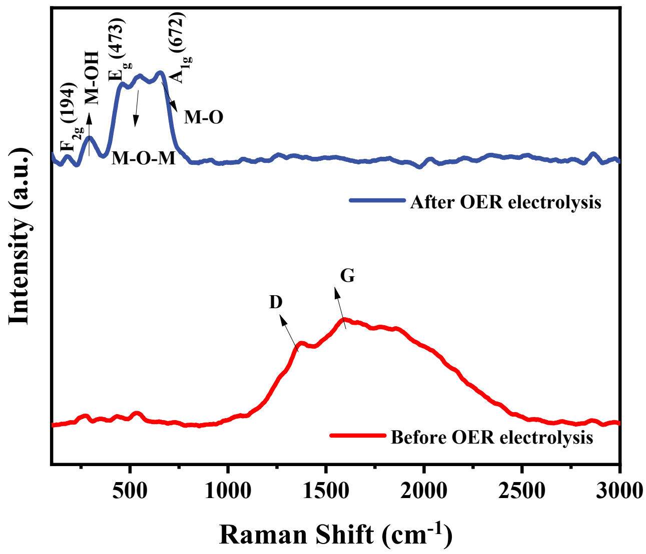

Figure S19. Raman spectra of NCFNF(433) before (a) and after (b) the OER testing. (Raman spectrum test conditions: the wavelength of the laser is 532nm, the output power is 1.5mW, the width of the slit is 50um, and the exposure time is 5s; the powder samples were tested at room temperature)

Table S1. EDS results of $NaCo_{1-x}Fe_xNi_xF_3$.

Catalysts	Atomic ratio (%)			
	Co	Fe	Ni	Co/Fe/Ni
NCF	1	0	0	1/0/0
NCFNF(811)	0.81	0.12	0.07	0.81/0.12/0.07
NCFNF(622)	0.61	0.21	0.18	0.61/0.21/0.18
NCFNF(433)	0.43	0.27	0.29	0.43/0.27/0.29

Table S2. ECSA results of $NaCo_{1-x}Fe_xNi_xF_3$ and RuO_2

Catalysts	ECSA for OER
NCF	1725 cm^{-2}
NCFNF(811)	2100 cm^{-2}
NCFNF(622)	2475 cm^{-2}
NCFNF(433)	2750 cm^{-2}
NCFF(73)	650 cm^{-2}
NCNF(73)	975 cm^{-2}
RuO_2	275 cm^{-2}

Table S3. The performance Comparison list of Perovskite-based electrocatalysts for OER.

Catalysts	η (mv) @10 mA cm^{-2}	Tafel slope (mVdec^{-1})	Stability	Ref.
NCFNF(433)	**265**	**49**	**100 h**	**This work**
$K_{0.8}Na_{0.2}(MgMnFeCoNi)F_3$	314	55	10 h	1
$SrCoO_{2.85-\delta}F_{0.15}$	420	60	20 h	2
$La(CrMnFeCo_2Ni)O_3$	325	51.2	50 h	3
$Sr_{0.95}Ce_{0.05}Fe_{0.9}Ni_{0.1}O_{3-\delta}$	340	51	30 h	4
$Sr_2Fe_{0.8}Co_{0.2}Mo_{0.65}Ni_{0.35}O_{6-\delta}$	340	56	5 h	5
$LaCoO_3$-80nm	490	69	--	6
$Sr_2Co_{1.5}Fe_{0.5}O_{6-\delta}$	318	44.8	9.7 h	7
$SrNb_{0.1}Co_{0.7}Fe_{0.2}O_{3-\delta}$	390	134	10 h	8
$BaCo_{0.7}Fe_{0.2}Sn_{0.1}O_{3-\delta}$	380	69	2 h	9
$La_5Ni_4O_{13-\delta}$	390	70	1000 cv	10
La_2NiMnO_6	370	58	12.5 h	11
F-$Ba_{0.5}Sr_{0.5}Co_{0.8}Fe_{0.2}O_{3-\delta}$	280	102	100 h	12
$PrBa_{0.5}Sr_{0.5}Co_{1.5}Fe_{0.5}O_{5+\delta}$	358	52	12 h	13
$La_{0.6}Sr_{0.4}Co_{0.8}Fe_{0.2}O_3$@$Ni_3(HITP)_2$	272	95	12 h	14
$SrCo_{0.95}P_{0.05}O_{3-\delta}$	290	52	1000 cv	15
$Ba_{0.5}Sr_{0.5}Co_{0.8}Fe_{0.2}O_{3-\delta}$	340	70	10 h	16
$Ba_2CoMo_{0.5}Nb_{0.5}O_{6-\delta}$	445	77	2 h	17

References

[S1] T. Wang, H. Chen, Z. Yang, J. Liang and S. Dai, High-Entropy Perovskite Fluorides: A New Platform for Oxygen Evolution Catalysis, J. Am. Chem. Soc., 2020, **142,** 4550-4554.

[S2] W. Wang, Y. Yang, D. Huan, L. Wang, N. Shi, Y. Xie, C. Xia, R. Peng and Y. Lu, An excellent OER electrocatalyst of cubic $SrCoO_{3-\delta}$ prepared by a simple F-doping strategy, J. Mater. Chem. A., 2019, **7,** 12538-12546.

[S3] T. X. Nguyen, Y. C. Liao, C. C. Lin, Y. H. Su and J. M. Ting, Advanced High Entropy Perovskite Oxide Electrocatalyst for Oxygen Evolution Reaction, Adv. Funct. Mater., 2021, **31,** 2101632.

[S4] S. She, Y. Zhu, X. Wu, Z. Hu, A. Shelke, W. F. Pong, Y. Chen, Y. Song, M. Liang, C. T. Chen, H. Wang, W. Zhou and Z. Shao, Realizing High and Stable Electrocatalytic Oxygen Evolution for Iron-Based Perovskites by Co-Doping-Induced Structural and Electronic Modulation, Adv. Funct. Mater., 2021, **32**, 2111091.

[S5] H. Sun, X. Xu, Z. Hu, L. H. Tjeng, J. Zhao, Q. Zhang, H.-J. Lin, C.-T. Chen, T.-S. Chan, W. Zhou and Z. Shao, Boosting the oxygen evolution reaction activity of a perovskite through introducing multi-element synergy and building an ordered structure, J. Mater. Chem. A., 2019, **7,** 9924-9932.

[S6] S. Zhou, X. Miao, X. Zhao, C. Ma, Y. Qiu, Z. Hu, J. Zhao, L. Shi and J. Zeng, Engineering electrocatalytic activity in nanosized perovskite cobaltite through surface spin-state transition, Nat. Commun., 2016, **7,** 11510.

[S7] S. R. Ede, C. N. Collins, C. D. Posada, G. George, H. Wu, W. D. Ratcliff, Y. Lin, J. Wen, S. Han and Z. Luo, Intermediate $Sr_2Co_{1.5}Fe_{0.5}O_{6-\delta}$ Tetragonal Structure between Perovskite and Brownmillerite as a Model Catalyst with Layered Oxygen Deficiency for Enhanced Electrochemical Water Oxidation, ACS. Catal., 2021, **11,** 4327-4337.

[S8] Y. Zhu, W. Zhou, Y. Zhong, Y. Bu, X. Chen, Q. Zhong, M. Liu and Z. Shao, A Perovskite Nanorod as Bifunctional Electrocatalyst for Overall Water Splitting, Adv. Energy. Mater., 2017, **7,** 1602122.

[S9] X. Xu, C. Su, W. Zhou, Y. Zhu, Y. Chen and Z. Shao, Co-doping Strategy for Developing Perovskite Oxides as Highly Efficient Electrocatalysts for Oxygen Evolution Reaction, Adv. Sci, 2016, **3,** 1500187.

[S10] S. R. Choi, J.-I. Lee, H. Park, S. W. Lee, D. Y. Kim, W. Y. An, J. H. Kim, J. Kim, H.-S. Cho and J.-Y. Park, Multiple perovskite layered lanthanum nickelate Ruddlesden-Popper systems as highly active bifunctional oxygen catalysts, Chem. Eng. J., 2021, **409,** 128226.

[S11] Y. Tong, J. Wu, P. Chen, H. Liu, W. Chu, C. Wu and Y. Xie, Vibronic Superexchange in Double Perovskite Electrocatalyst for Efficient Electrocatalytic Oxygen Evolution, J. Am. Chem. Soc., 2018, **140,** 11165-11169.

[S12] J. Xiong, H. Zhong, J. Li, X. Zhang, J. Shi, W. Cai, K. Qu, C. Zhu, Z. Yang, S. P. Beckman and H. Cheng, Engineering highly active oxygen sites in perovskite oxides for stable and efficient oxygen evolution, Appl. Catal., B, 2019, **256,** 117817.

[S13] B. Zhao, L. Zhang, D. Zhen, S. Yoo, Y. Ding, D. Chen, Y. Chen, Q. Zhang, B. Doyle, X. Xiong and M. Liu, A tailored double perovskite nanofiber catalyst enables ultrafast oxygen evolution, Nat. Commun., 2017, **8,** 14586.

[S14] Z. Li, J.-G. Li, X. Ao, H. Sun, H. Wang, M.-F. Yuen and C. Wang, Conductive metal–Organic frameworks endow high-efficient oxygen evolution of La0·6Sr0·4Co0·8Fe0·2O3 perovskite oxide nanofibers, Electrochim. Acta, 2020, **334,** 135638, DOi: 10.1016/j.electacta.2020.135638

[S15] Y. Zhu, W. Zhou, J. Sunarso, Y. Zhong and Z. Shao, Phosphorus-Doped Perovskite Oxide as Highly Efficient Water Oxidation Electrocatalyst in Alkaline Solution, Adv. Funct. Mater., 2016, **26,** 5862-5872.

[S16] G. Chen, W. Zhou, D. Q. Guan, S. Jaka, Y. P. Zhu, X. F. Hu and W. S. Zhang, Z.P., Two orders of magnitude enhancement in oxygen evolution reactivity on amorphous $Ba_{0.5}S_{r0.5}Co_{0.8}Fe_{0.2}O_{3-\delta}$ nanofilms with tunable oxidation state, Sci. Adv., 2017, **3,** e1603206.

[S17] H. Sun, G. Chen, J. Sunarso, J. Dai, W. Zhou and Z. Shao, Molybdenum and Niobium Codoped B-Site-Ordered Double Perovskite Catalyst for Efficient Oxygen Evolution Reaction, ACS Appl. Mater. Interfaces, 2018, **10,** 16939-16942.